


# Artificial neural network and associated computer tool for rapid shear strength prediction of two-span continuous deep beams

Prativa Pathak, Serhan Guner<sup>\*</sup> 

Department of Civil and Environmental Engineering, The University of Toledo, Toledo, OH 43607, USA

## ARTICLE INFO

### Keywords:

Artificial neural network  
Computer tool  
Continuous deep beams  
SHapley Additive exPlanations analysis  
Shear behavior  
Shear strength

## ABSTRACT

Continuous deep beams exhibit complex shear behavior due to non-linear strain distribution and coexistence of high shear and high moment within the same regions. This behavior makes it challenging to predict their shear strength accurately. The objective of this study is to develop a pioneering artificial neural network and associated computer tool to accurately and rapidly predict the shear strength of two-span continuous deep beams. Literature lacks machine learning algorithms specifically developed for continuous deep beams. To achieve this objective, a comprehensive database of 150 experimental specimens is compiled from eight previously published research studies. The 140 data points, which passed the exploratory data analysis, are used to train, validate, and test the proposed network for applicability to a wide range of input parameters. The accuracy and reliability of the proposed network are evaluated using a comprehensive set of evaluation metrics including the correlation coefficient (R), determination coefficient ( $R^2$ ), mean absolute error (MAE), mean squared error (MSE), root mean squared error (RMSE), and the coefficient of variation (CV). The importance of the input parameters on the predicted shear strength is evaluated using the SHapley Additive exPlanations analysis. Another important objective is to develop an open-access computer tool to execute network formulations and rapidly calculate the shear strengths of continuous deep beams. The computer tool aims to bridge the gap between research and practice and enable the use of the developed network for continuous beam when there are no experimental testing results available.

## 1. Introduction

Reinforced concrete deep beams are structural elements commonly used in transfer girders and lower floors of high-rise buildings, foundation elements such as pile caps, and bridge elements such as pier caps (e.g., Fig. 1). The most common parameter used to characterize deep beams is the shear span-to-depth ratio ( $a/d$ ), where the shear span ( $a$ ) is the distance from the load to the center of the corresponding support, and the depth ( $d$ ) is the distance from the extreme compression fiber to the centroid of the tension reinforcement. As illustrated in Fig. 2, beams with lower  $a/d$  ratios (typically  $\leq 2.0$ ) behave as deep beams, while those with higher  $a/d$  ratios ( $\geq 3.0$ ) behave as slender beams and are analyzed using the sectional method. Between these extremes lies a transition zone ( $2.0 < a/d < 3.0$ ), where the behavior is governed by both arching and flexural actions. Design codes [1–4] typically define deep beams based on the  $a/d$  ratio being less than or equal to either 2.0 or 2.5.

Deep beams, both simply supported and continuous, are

characterized by non-linear strain distribution and are prone to brittle shear failure mechanisms. Continuous deep beams present additional challenges, including high shear forces and negative bending moments in the same interior shear span, typically near an intermediate support. This influences diagonal crack development and adversely affects the efficiency of interior struts [6]. In contrast, large shear force occurs in low bending moment region of simply supported deep beams [7]. Additionally, in the failed shear span of simply supported beams, the diagonal cracks tend to form below the critical shear crack while in continuous beams cracks develop on both sides of critical shear crack (e.g. Fig. 3) [7]. Furthermore, the statically indeterminate nature and higher stiffness of continuous deep beams make them particularly sensitive to differential support settlements. Even small displacements at supports introduce additional moments and shear forces, affecting crack initiation and propagation patterns [8]. All these complex behaviors of continuous deep beams make their shear strength calculation challenging.

Shear strength of continuous deep beams is influenced by many

<sup>\*</sup> Corresponding author.

E-mail addresses: [prativa.pathak@rockets.utoledo.edu](mailto:prativa.pathak@rockets.utoledo.edu) (P. Pathak), [serhan.guner@utoledo.edu](mailto:serhan.guner@utoledo.edu) (S. Guner).

<https://doi.org/10.1016/j.istruc.2025.109956>

Received 3 July 2025; Accepted 11 August 2025

Available online 18 August 2025

2352-0124/© 2025 The Author(s). Published by Elsevier Ltd on behalf of Institution of Structural Engineers. This is an open access article under the CC BY-NC-ND license (<http://creativecommons.org/licenses/by-nc-nd/4.0/>).

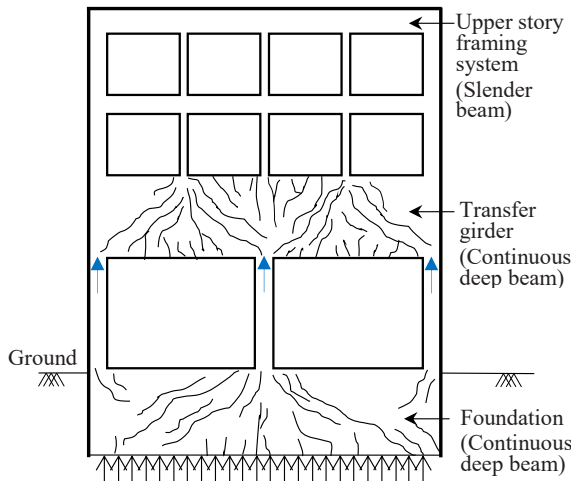


Fig. 1. Sample building structure with deep beams.

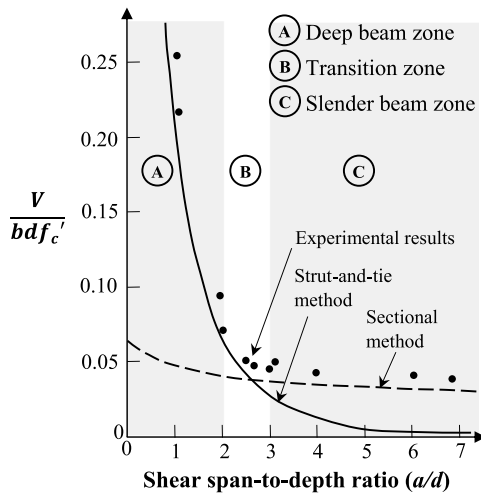
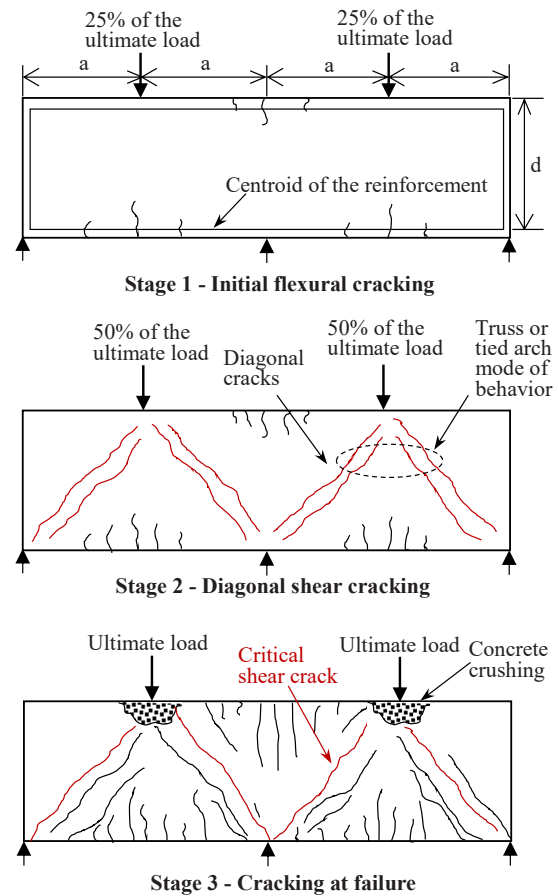


Fig. 2. Variation of shear strength across various ranges of  $a/d$  ratios (adopted from [5]).

interacting parameters which further complicate its accurate calculation. Several methods have been proposed to calculate the shear strength of deep beams. Among these, the Strut-and-Tie Method (STM) is the most widely used method and recommended by design codes such as ACI 318–25 [1], AASHTO LRFD [2], CSA A23.3 [3], and IS 456 [4]. STM idealizes the internal force flow through a truss-like system of compression struts and tension ties intersecting at nodes. While STM provides a rational and accurate analysis method for deep beams (e.g. Fig. 2) [1–5,10], the detailed equations and geometrical rules for creating valid strut-and-tie models require expert level knowledge and an iterative solution specific to each problem being modeled [11]. In addition, there is a scarcity of computer tools that can create and analyze valid strut-and-tie models for a given problem.

Given these challenges, machine learning (ML) can provide a promising solution to predict the shear strength of deep beams through a self-learning process based on existing experimental results. Recent advances in ML algorithms, including artificial neural networks, support vector machines, random forests, and gradient boosting techniques, offer promising solutions for capturing such complex behavioral patterns. ML algorithms have been successfully applied to predict the shear strength of slender beams [12–14], columns [15,16], beam-column joints [17–19], and the load capacity of anchors [20]. For the shear strength prediction of deep beams, ML algorithms are only focused on the simply supported beams [21–28]. Research efforts applying ML



**Note:** Crack patterns are schematic and shown for reference only. Actual crack development may vary between specimens. Non-symmetrical, single discrete, or localized cracking are also common.

Fig. 3. Typical cracking behavior of continuous deep beams (adopted from [9]).

algorithms to continuous deep beams are lacking, despite their practical significance.

In this study, Artificial Neural Networks (ANNs) are adopted to predict the shear strength of continuous deep beams. Since shear strength in deep beams depend on many interacting parameters and their relations are non-linear and complex, ANNs are well-suited to capture these relationships accurately. The effectiveness of ANN in solving complex problems has been demonstrated in several studies which reinforce its suitability for the purpose of this study. Goh [21] applied the artificial neural network (ANN) to predict slender beam shear strength. In a subsequent study, Sanad and Saka [22] verified the effectiveness of ANN in predicting the shear strength of deep beam. Nyugen et al. [23] recently compared performance of seven ML algorithms and concluded that ANN, ensemble of trees, gradient boosting, and Gaussian process regression exhibited superior performance to predict shear strength of simply supported deep beams. The results show that ANN provides an effective solution in accurately predicting the shear strength of deep beams. Additionally, ANNs allow for relatively straightforward implementation in user-oriented tools for seamless application in engineering practice without requiring specialized ML software. One weakness that is noted in this literature review is the lack of computer tools that can execute the proposed ML algorithms in most studies. It is challenging, and sometimes impossible, to analyze a beam other than those considered in the study and predict its shear strength. This defeats the purpose of developing a predictive network.

This research aims to develop a pioneering artificial neural network

and associated computer tool for the accurate, reliable, and rapid shear strength prediction of the two-span continuous deep beams. The artificial neural network is developed using a comprehensive database with a large range of applicability and derived exclusively from the experimental tests of two-span continuous deep beams. The associated computer tool, named ANN-ConDeep, aims to transfer the research findings into practical application, allowing the engineering community to predict the shear strength of two-span continuous deep beams with no experimental results.

## 2. Development of the artificial neural network (ANN)

### 2.1. Background

An Artificial neural network (ANN) is a computational tool inspired by the architecture, functional operations, and operating features of the biological neural system. It consists of interconnected processing units called neurons, which modify themselves based on the information passing through them, mimicking the learning process of biological neurons (Fig. 4).

Each neuron receives multiple input signals ( $I_1, I_2, \dots, I_N$ ), which are individually weighted ( $W_1, W_2, \dots, W_N$ ). Weights are scalar values that define the strength of connections between neurons, determining how much influence one neuron's output has on another. Additionally, each neuron has an associated bias, a constant that allows the network to adjust and fine-tune its predictions. The neurons compute the weighted sum of the inputs, which are the outputs of each layer. The weighted sum of the input is mathematically derived using Eq. (1):

$$n = \sum_{i=1}^N I_i W_i + b \quad (1)$$

where  $I_i$  are the input signals to the neuron,  $W_i$  are the weights associated with each input, and  $b$  is the bias. This weighted sum,  $n$ , is then passed through an activation function, such as Rectified Linear Unit (ReLU), tanh, sigmoid, or linear, which converts the weighted sum into the neuron's output signal. The ReLU activation function has shown to be highly effective for regression and classification purposes [29] and thus used in this study. The ReLU function is defined as in Eq. (2):

$$f(n) = \max(0, n) \quad (2)$$

The output of each neuron is then transmitted to neurons in subsequent layers, where it is further processed by additional weights and biases, ultimately reaching the output layer. This process is known as forward propagation. After the forward propagation, the error between the predicted ( $V_{pred}$ ) and experimental values ( $V_{exp}$ ) for  $m$  data points is calculated using loss functions, such as the mean squared error, as defined in Eq. (3).

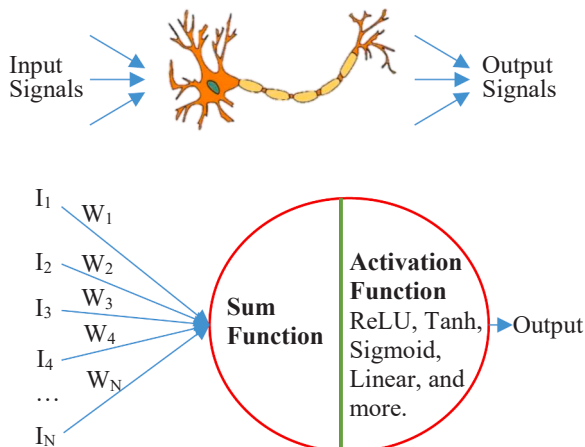


Fig. 4. Mechanism of an artificial neuron depicting a biological neuron.

$$MSE = \frac{1}{m} \sum (V_{exp} - V_{pred})^2 \quad (3)$$

The gradient of this loss function is then used to adjust the weights and biases in the network to minimize prediction errors. This process is known as backward propagation. This iterative process continues until the network reaches an optimal state where prediction errors are minimized.

### 2.2. Experimental database

The experimental database compiled in this study includes two-span continuous deep beams subjected to two equal point loads ( $P$ ) acting symmetrically with respect to the centerline. The basic parameters that influence the shear strength include the width of the beam ( $b_w$ ), the effective depth of the beam ( $d$ ), the shear span-to-depth ratio ( $a/d$ ), the compressive strength of concrete ( $f_c'$ ), the yield strength of longitudinal and transverse reinforcement ( $f_{yh}$  and  $f_{yv}$ ), the longitudinal top and bottom reinforcement ratio ( $\rho_h'$  and  $\rho_h$ ), the transverse reinforcement ratio ( $\rho_v$ ), the width of loading plate ( $l_l$ ), and, the width of support plate ( $l_s$ ) – all shown in Fig. 5.

From eight different research studies [8,9,30,31–35], a total of 150 experimental results have been collected (see Appendix A). Every effort is made to identify all available experimental results with intended beam and loading configuration. The experimental database covers the beams with various  $a/d$  ratios from 0.54 to 2.67. 81 specimens have  $a/d$  ratios less than 2.0, and 69 specimens have  $a/d$  ratios ranging from 2.02 to 2.67. This range captures both the deep beam ( $a/d < 2$ ) and the transition zone ( $2 < a/d < 3$ ) behaviors. All specimens exhibited shear-critical behaviors in the experiments.

Table 1 shows the ranges of input parameters in the database. The wide range of parameters is essential to generalize the use of the network because ANNs are not appropriate for the extrapolation of data. Any deep beam that will be analyzed by the network should have the input parameters in these ranges.

The distribution of the input parameters across various ranges in the database is shown in Fig. 6. An even distribution of the data points across each parameter suggests good data distribution. The frequency distribution assessment conducted on the input parameters of the experimental database shows that the parameters captured an acceptable range for the network to be accurate in predicting the shear strength.

### 2.3. Exploratory data analysis

Exploratory Data Analysis (EDA) is performed to identify potential outliers and understand the relationship between parameters before using the database for the development of a network. As part of this

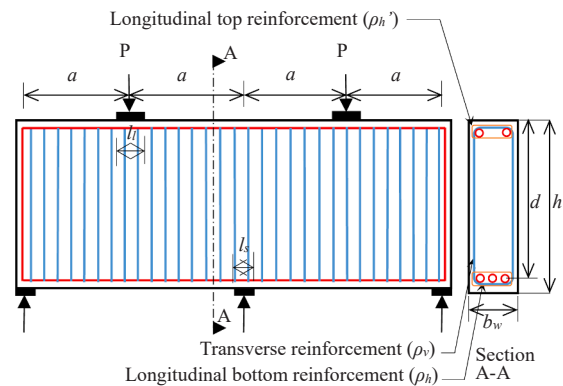


Fig. 5. Basic parameters for the shear strength prediction of the two-span continuous deep beam.

**Table 1**

Range of input parameters in the database.

Input parameters	Min	Max	Unit
Width of beam ( $b_w$ )	120	200	mm
Effective depth of beam ( $d$ )	381	1000	mm
Shear span-to-depth ratio ( $a/d$ )	0.54	2.67	-
Compressive strength of concrete ( $f_c'$ )	14.5	68.2	MPa
Yield strength of longitudinal reinforcement ( $f_{yh}$ )	285	586	MPa
Yield strength of transverse reinforcement ( $f_{yv}$ )	347	581	MPa
Longitudinal top reinforcement ratio ( $\rho_h$ )	0.32	4.86	%
Longitudinal bottom reinforcement ratio ( $\rho_b$ )	0.32	4.76	%
Transverse reinforcement ratio ( $\rho_v$ )	0.15	0.84	%
Width of loading plate ( $l_l$ )	150	300	mm
Width of support plate ( $l_s$ )	160	400	mm

process, an outlier detection is performed using Cook's distance to remove any influential data points or outliers that negatively affect the network performance, followed by correlation coefficient analysis to

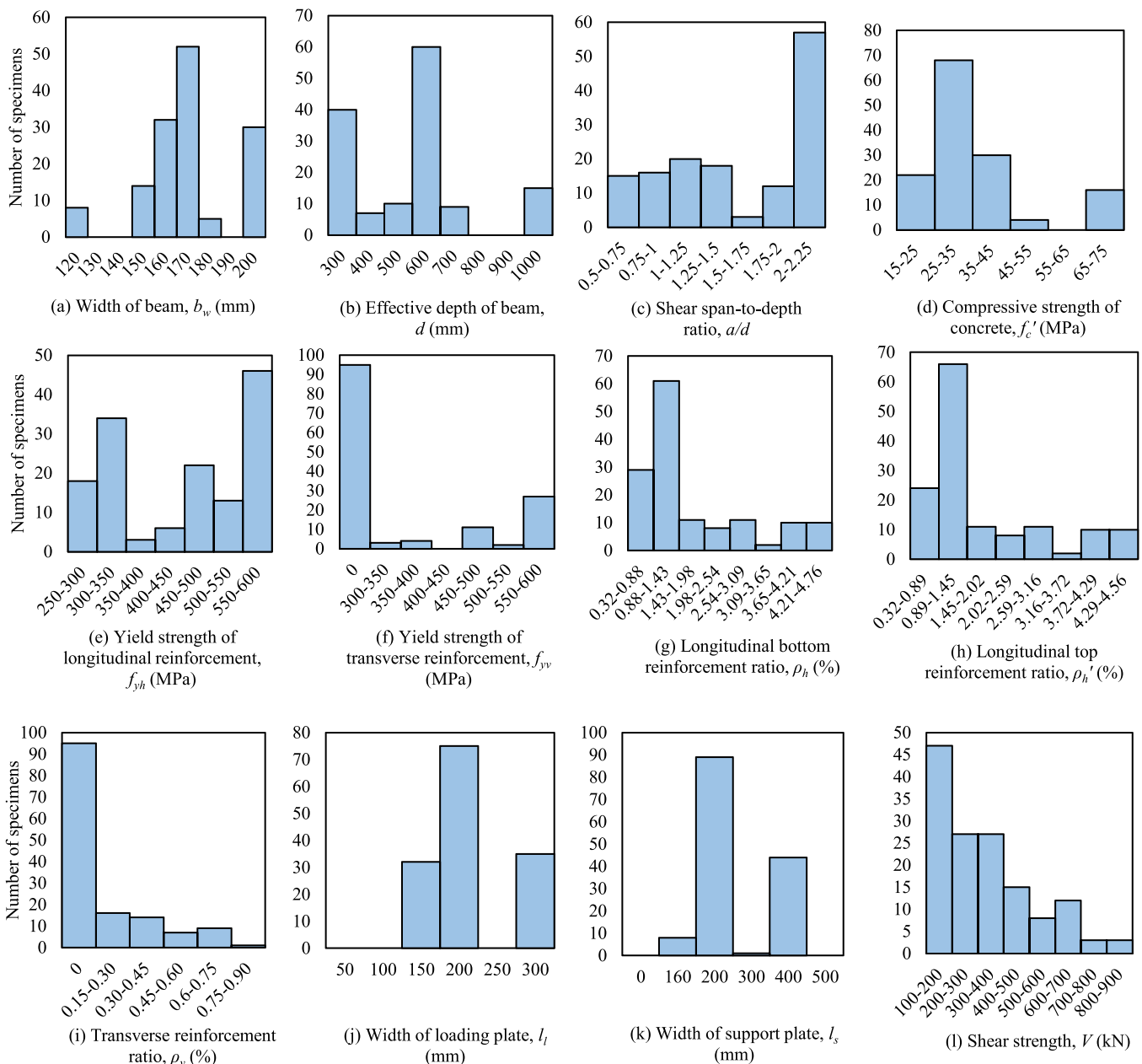
assess the relationships between parameters.

Cook's distance is a statistical method used to estimate the influence of a data point when performing the least squares regression analysis. The general idea behind Cook's distance is to measure how much the regression coefficients would change if a particular data point were removed from the database. The formula to calculate the Cook's distance for the  $i^{th}$  observation is expressed below in Eq. (4). Any data point with Cook's distance greater than the threshold limit ( $I_t$ ) in Eq. (5) is considered an outlier and should be removed from the database.

$$D_i = \left( \frac{r_i^2}{p \cdot MSE} \right) \cdot \left( \frac{h_{ii}}{(1 - h_{ii})^2} \right) \quad (4)$$

$$I_t = \frac{4}{m} \quad (5)$$

where  $r_i$  is the  $i^{th}$  residual (i.e., residual for the  $i^{th}$  observation),  $p$  is the number of coefficients in the regression network, MSE is the mean squared error,  $h_{ii}$  is the  $i^{th}$  leverage value, and  $m$  is the total number of

**Fig. 6.** Distribution of input and output parameters in the experimental database.

data points in the database.

The results of outlier detection using Cook's distance are shown in Fig. 7. The data lying above the threshold value of  $I_t$  equal to 0.0267 are outliers. After the application of the Cook's distance method, 10 specimens were identified as outliers and removed from the database, leaving an experimental database of 140 specimens for the network creation.

After removing the outliers from the experimental database, the correlation coefficient analysis is performed to quantify the correlation between the input and output parameters using Eq. (6) where  $r_{xy}$  is the correlation coefficient,  $m$  is the sample size,  $x_i$  and  $y_i$  are the individual sample points for the input and output parameters respectively indexed with  $i$ , and  $\bar{x}$  and  $\bar{y}$  are the average values for the input and output parameters, respectively.

$$r_{xy} = \frac{\sum_{i=1}^m (x_i - \bar{x})(y_i - \bar{y})}{\sqrt{\sum_{i=1}^m (x_i - \bar{x})^2} \cdot \sqrt{\sum_{i=1}^m (y_i - \bar{y})^2}} \quad (6)$$

The correlation between the input parameters and the shear strength is more clearly expressed using a heatmap as shown in Fig. 8. The input parameters include  $b_w$ ,  $d$ ,  $a/d$ ,  $f_c'$ ,  $f_{yh}$ ,  $f_{yv}$ ,  $\rho_h$ ,  $\rho_h'$ ,  $\rho_v$ ,  $l_b$  and  $l_s$ . The correlation coefficients range from +1 to -1, where +1 indicates a strong direct correlation between the parameters, 0 indicates no relationship between the parameters, and -1 indicates a strong inverse correlation between the parameters. For instance, the correlation coefficient between the shear span-to-depth ratio ( $a/d$ ) and the shear strength ( $V$ ) is -0.74, indicating a strong negative correlation of 74 %. This indicates that as the shear span-to-depth ratio increases, the shear strength decreases, and vice versa. Similarly, the correlation coefficient between the compressive strength of concrete ( $f_c'$ ) and the shear strength ( $V$ ) is 0.43, indicating a positive correlation of 43 %.

The beam width, the width of loading, and the width of support plates have lower correlation values of -0.02, 0.13, and 0.28, respectively, with the shear strength as compared to the other eight input parameters. While the width of a beam does affect the cross-sectional area available to resist shear forces, its impact is relatively minor compared to other factors such as the shear span-to-depth ratio and effective depth. The primary function of the loading plate is to ensure that the load is applied uniformly, which helps in avoiding localized failures under the plate, without significantly affecting the shear strength. The support plate affects the distribution of reaction forces at the support. While the support plate can affect the bearing capacity and prevent local crushing at the supports, it has a limited effect on the overall shear strength of the beam as demonstrated in the heatmap.

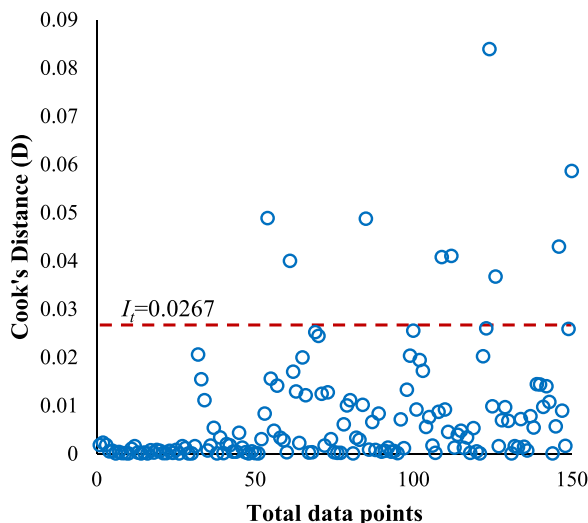


Fig. 7. Outlier detection using Cook's distance method.

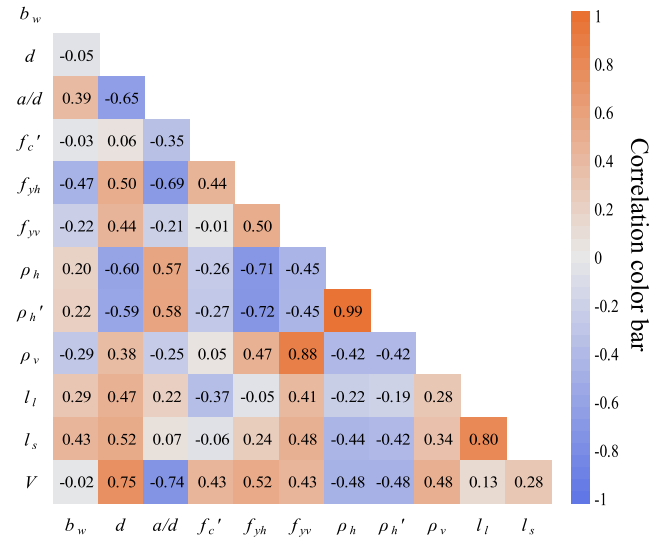


Fig. 8. Correlation coefficient analysis between input parameters and shear strength.

#### 2.4. Network architecture

The main components of the network architecture include activation functions, optimization functions, learning rate, and network configurations. The rectified linear unit function (ReLU) is selected in this study as the activation function for the hidden layer because of its capability to discard neurons with negative weights and biases in the learning process, allowing for a faster and more precise learning process [36].

Adaptive moment estimation (Adam) with a learning rate ( $k$ ) of 0.1 is selected as an optimization function to update the weights and biases. Adam optimization function allows the weights and biases to converge to optimum values with less iterations (i.e., faster) while providing more accurate shear strength predictions. The selection of the learning rate as 0.1 is based on parametric study. The validation loss of the network is computed for the network with different learning rates, i.e., 0.001, 0.01, and 0.1, for 20 trials. For the maximum trials, the validation loss is found to be converged within values around 0.286 for the learning rate 0.1, whereas for the learning rates 0.001 and 0.01, the validation losses are converged within 0.985 and 0.445, respectively. Hence, the learning rate with lower validation loss, i.e., 0.1, is selected.

In addition, a parametric study is conducted to find an efficient network configuration. To achieve this, the accuracy of the various network configurations is evaluated based on the mean squared error. All these configurations consist of one input layer with eleven neurons and one output layer with one neuron, while the number of neurons in the hidden layer is varied from 1 to 50, and their accuracy is checked. The network configuration with the least mean squared error is then selected as the most efficient configuration. The MSEs computed for configurations are shown in Fig. 9, where the most efficient network configuration is found for a hidden layer with twenty-eight neurons.

The final configuration of the network is presented in Fig. 10. It consists of one input layer with eleven neurons, one hidden layer with twenty-eight neurons, and one output layer with one neuron. The eleven neurons in the input layer are the eleven input parameters, and one neuron in the output layer is the shear strength of a two-span continuous deep beam ( $V_{pred}$ ).

The predicted shear strength ( $V_{pred}$ ) is the nominal (unfactored) shear strength of a two-span continuous deep beam with equal point loads ( $P$ ) at the center of each span. The relationship between the point loads ( $P$ ) and the shear strength ( $V_{pred}$ ) of a beam can be calculated using statics. For a two-span continuous beam with equal point loads on two spans, the statics require that the point load ( $P$ ) at the center of each



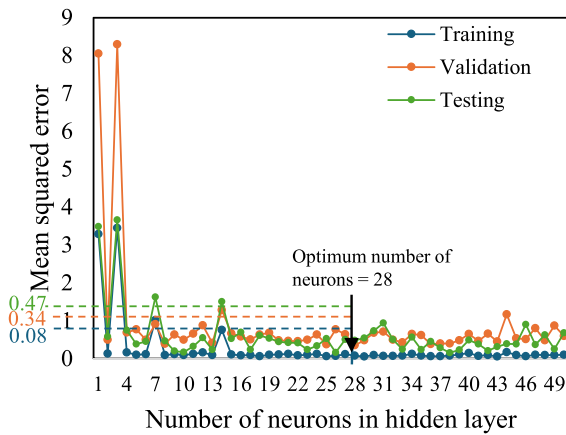


Fig. 9. MSEs computed for various network configurations.

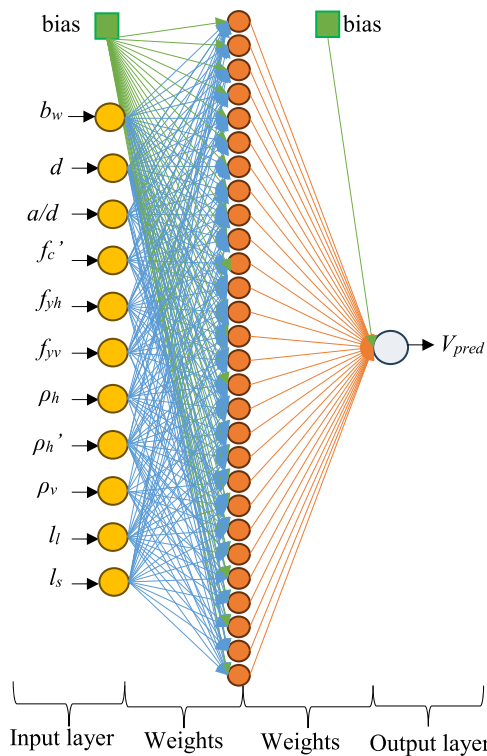


Fig. 10. Schematic representation of the proposed network.

span is equal to 16/11 times the shear strength ( $V_{pred}$ ). The predicted shear strength should be multiplied by the strength reduction factor according to applicable design codes to obtain the factored shear strength. For example, the strength reduction factors recommended by ACI 318–25 [1], AASHTO LRFD [2], and CSA A23.3–2024 [3] are 0.75, 0.75, and 0.65, respectively.

## 2.5. Network training, validation, and testing

Using 140 data points, which passed the exploratory data analysis, the final network configuration is trained, validated, and tested. For that, the database is split into 80 % training sets, 10 % validation sets, and 10 % testing sets. Before training the network, all the input parameters of the database are standardized to a similar scale using the StandardScaler tool [37]. This standardization involves calculating the mean and standard deviation for each input parameter across the training sets. Each input parameter is then transformed by subtracting

the mean and dividing by the standard deviation, resulting in standardized values with a mean of 0.00 and a standard deviation of 1.00. This step allows all input parameters to contribute equally to the network training.

The training of the network is then carried out with the training set while monitoring its accuracy on the validation set. The forward propagation and backward propagation are applied to each input data of the training sets. To prevent the network from overfitting, the training of the network is halted if the validation loss does not improve for 50 epochs.

Following the training process, the testing of the network is carried out by performing the forward propagation and computing the error for all data points of the testing sets. The accuracy and reliability of the proposed network are evaluated using six different evaluation metrics, including R,  $R^2$ , MAE, MSE, RMSE, and CV. R is the correlation coefficient defined in Eq. (7), which is used to evaluate the correlation between the predicted and experimental shear strength values  $V_{pred}$  and  $V_{exp}$ . R ranges from 0 to 1, where 1 indicates the highest correlation.  $R^2$  is the determination coefficient defined in Eq. (8), which indicates the extent to which the predicted value matches the experimental value regardless of their direction.  $R^2$  ranges from 0 to 1, where 1 indicates the best fit.

$$R = \frac{m \sum V_{exp} V_{pred} - (\sum V_{exp})(\sum V_{pred})}{\left[ m \sum V_{exp}^2 - (\sum V_{exp})^2 \right] \left[ m \sum V_{pred}^2 - (\sum V_{pred})^2 \right]} \quad (7)$$

$$R^2 = 1 - \frac{\sum (V_{exp} - V_{pred})^2}{\sum (V_{exp} - \bar{V}_{pred})^2} \quad (8)$$

MAE is the mean absolute error defined in Eq. (9), which is the average error between the predicted and experimental values. MSE is the mean squared error defined in Eq. (3), which is the average squared difference between predicted and experimental values. RMSE is the root mean squared error defined in Eq. (10), which is the average magnitude of the errors between predicted and experimental values. CV is the coefficient of variation defined in Eq. (11), which is the ratio of the standard deviation to the mean. For the error metrics (MAE, MSE, and RMSE) and CV, smaller numbers indicate more accurate results.

$$MAE = \frac{1}{m} \sum |V_{exp} - V_{pred}| \quad (9)$$

$$RMSE = \sqrt{\frac{1}{m} \sum (V_{exp} - V_{pred})^2} \quad (10)$$

$$CV = \frac{RMSE}{\frac{1}{m} \sum V_{pred}} \times 100 \quad (11)$$

The values of these metrics for the training, validation, and testing sets are provided in Table 2. The R and  $R^2$  values closer to 1 indicate a strong relationship between the predicted and experimental values and a good fit of the network. The network achieved R values above 0.96 and  $R^2$  values above 0.92 across all data splits. The lower values of RMSE, MSE, and MAE indicate that the network can give predicted values close to the experimental values, making it reliable for the prediction of the shear strength of the two-span continuous deep beams.

To visually assess the quality of predictions, the ANN predictions of

Table 2

Evaluation metrics for training, validation, and testing sets.

Evaluation Metrics	Training	Validation	Testing
R	0.98	0.96	0.98
$R^2$	0.97	0.92	0.97
MAE	21.68	26.75	32.05
MSE	949.76	1395.52	1702.28
RMSE	30.82	37.36	41.26
CV	9.65 %	10.89 %	9.85 %

the shear strength ( $V_{pred}$ ) of training, validation, and testing set versus the experimental values of the shear strength of the experimental data ( $V_{exp}$ ) are plotted in Fig. 11. In these plots, an ideal result where the network predicts exactly the experimental results, would be a  $y = x$  line with  $R^2$  value closer to 1, which is close to the graph obtained in the training process (Fig. 11a). As shown in Fig. 11b and Fig. 11c, the accuracy in the validation and testing set is similar to that in the training, with the coefficient of variation of 10.89 % and 9.85 %, and a slightly more inclined trendline ( $y = 1.04x$  and  $y = 0.99x$ ). The  $R^2$  values for the training, validation, and testing sets are 0.97, 0.92, and 0.97, respectively, and the R values are 0.98, 0.96, and 0.98, respectively. The average predicted-experimental shear strength ratios for 140 specimens are 1.00, with a coefficient of variation of 10.12 %. These results demonstrate the predictive accuracy of the proposed network.

Fig. 12 presents the scatterplots of the predicted-to-experimental shear strength ratios of the proposed network across the complete ranges of each input parameter. In these plots, the ideal ratio, where the network predictions are exactly equal to the experimental values, is shown with a horizontal line at 1.0. The predicted-to-experimental shear strength ratios, along with the mean and coefficient of variation, are presented in Appendix A.

The predictions of the proposed network for all eleven input parameters are closer to line 1.0 with less scatter and without visible bias. The predictions obtained from the proposed network provide significantly better agreement with the experimental results, regardless of the range of the input parameters.

To further analyze the results from the proposed network, the analysis results are presented in a box plot in Fig. 13, where the x-axis represents the range of input parameters, and the y-axis represents the predicted-to-experimental shear strength ratios ( $V_{pred}/V_{exp}$ ). These box plots include key statistical measures such as the interquartile range (IQR), median, mean, maximum, and minimum values. A smaller IQR indicates a low variability and high reliability in predictions. When the mean and median are close to each other, it implies a minimal influence of the outliers and a symmetric distribution of predictions.

The proposed network shows a mean and median value closer to 1.0 and significantly narrower IQR, indicating accurate and reliable predictions. For instance, in Fig. 13c, for various ranges of the shear span-to-depth ratio ( $a/d$ ), the proposed network maintains the mean and median values close to 1.0, and relatively small interquartile ranges (IQR approximately equal to 0.2). Similarly, in Fig. 13d, for various ranges of the compressive strength of concrete ( $f'_c$ ), the proposed network maintains the mean and median consistently close to 1.0 and narrow interquartile ranges from 0.98 to 1.1. For all eleven input

parameters, the proposed network consistently provides accurate and reliable predictions, with the mean and median values close to 1.0 and narrow interquartile ranges across all input parameter ranges.

Given the lack of ML algorithms for continuous deep beams, it is not possible to compare the proposed network with any ML algorithms from the literature. It is still desired to put the proposed ANN in the context of studies available in the literature. For this, a comparison study is performed with the ML algorithms developed for simply supported deep beams, and the results are presented in Table 3.

As shown in Table 3, the proposed network achieves an  $R^2$  of 0.97, which is higher than those reported by Nguyen et al. [23] and Feng et al. [25] and is comparable to Wang [24] and Cheng [27]. The coefficient of variation (CV) for the proposed network is 9.85 %, indicating lower relative dispersion of the prediction errors compared to Nguyen et al. [23] and Gandomi et al. [26], while remaining within a similar range as Feng et al. [25] and Cheng et al. [27]. In terms of error metrics, the proposed network achieved an MAE of 32.05 kN and RMSE of 41.26 kN, outperforming Nguyen et al. [23] and Gandomi et al. [26], producing results similar to those of Feng et al. [25], and falling short of Wang [24] and Cheng et al. [27]. These discrepancies may be considered insignificant given the experimental shear strengths in the database range widely from 103 kN to 875 kN. This comparison demonstrates that the proposed network provides comparable prediction accuracy to those available in the literature for simply supported deep beams, despite the fact that continuous deep beams exhibit more complex behaviors, which are significantly more challenging to predict.

### 3. Feature importance analysis

The neural networks can accurately learn complex, non-linear relationships and provide accurate predictions. However, their decision-making processes are difficult to interpret, which is why they are commonly referred to as “black box” models [25]. To better understand the predictions of the proposed network and gain confidence in the network’s predictive results, SHAP (SHapley Additive exPlanations) feature importance analysis is used in this study. SHAP analysis is a cooperative game-theory-based method that explains a network’s predictions by assigning a value to each input parameter based on its contribution to the network’s predictive results. The input parameters with higher SHAP values have a greater impact on the output of the network.

It is important to distinguish the SHAP analysis from the correlation coefficient analysis. While the correlation coefficient analysis measures the linear relationship between two parameters, the SHAP analysis

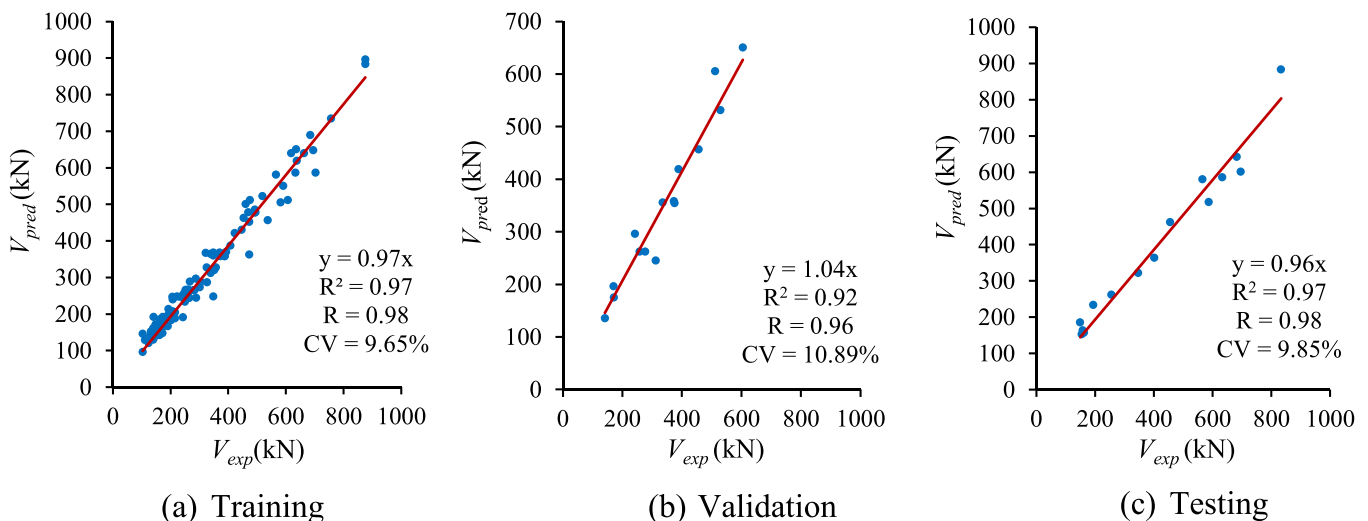


Fig. 11. Scatterplots of the predicted-to-experimental shear strength.

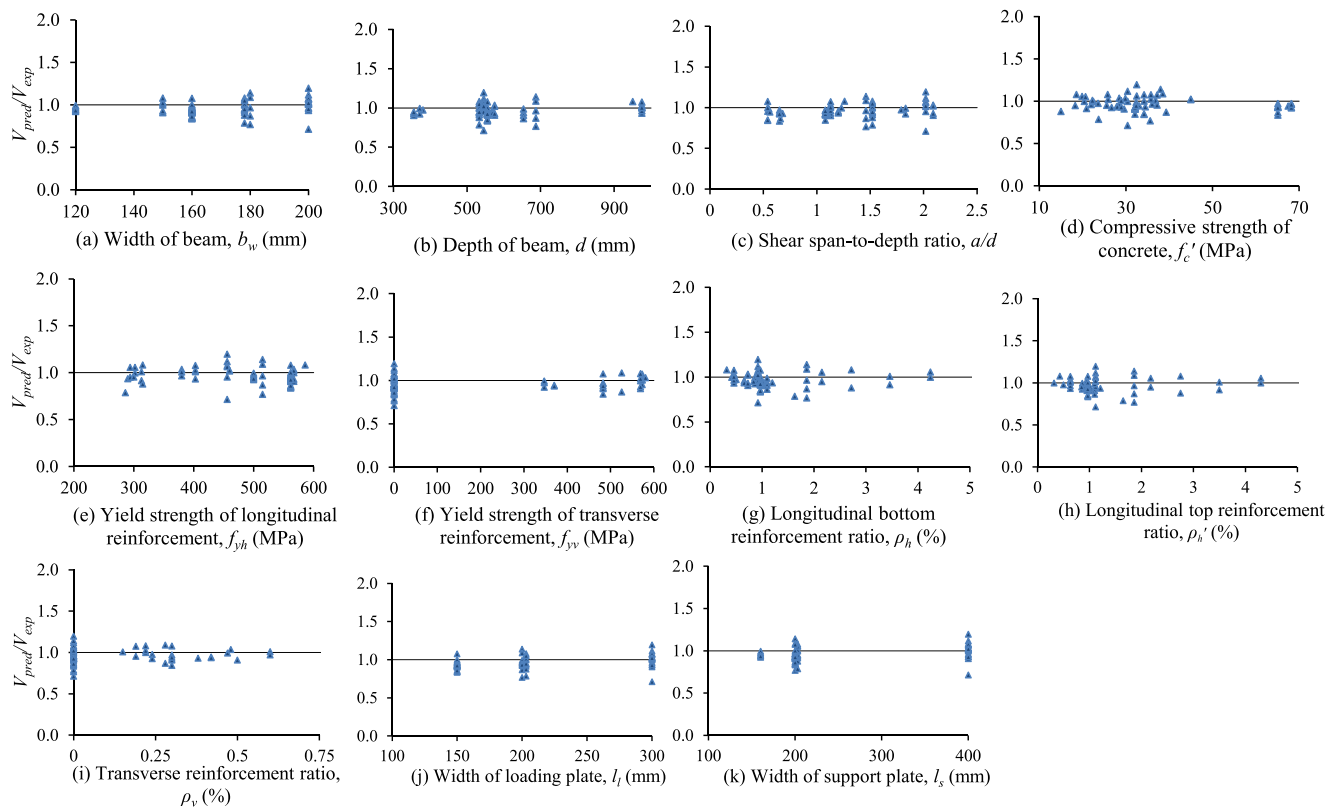


Fig. 12. Scatterplots of the predicted-to-experimental shear strength across various input parameter ranges.

provides a more comprehensive view of the importance of features in the context of a network's predictions. SHAP values explain how each feature contributes to the network's prediction and offer detailed explanations of the feature importance based on the learned network, whereas the correlation coefficients indicate the strength and direction of a linear relationship based on the experimental database.

The results of the feature importance analysis using SHAP are presented in Fig. 14, where the y-axis represents the input parameters ranked by the order of their importance in the network's prediction, and the x-axis represents their respective SHAP values. The SHAP summary plot in Fig. 14a shows the positive and negative impacts of the input parameters on the desired output and the most important parameters. In this case, the larger the shear span-to-depth ratio ( $a/d$ ), the more significant the negative impact on the shear strength, whereas the concrete compressive strength ( $f'_c$ ) positively affects the results. This result agrees well with the findings obtained from the correlation coefficient analysis and the previous experimental and modeling studies [38,39], suggesting that the network has captured meaningful structural relationships and learned the underlying patterns correctly. The SHAP bar plot in Fig. 14b further quantifies the mean absolute SHAP values for each feature, confirming that  $a/d$  has by far the greatest overall impact on the network's output.

#### 4. Development of a computer tool

To execute the network formulations and calculate the shear strength, an open-access computer tool, ANN-ConDeep: Artificial Neural Network for Continuous Deep Beams [40], is developed using a Microsoft Excel spreadsheet and shared as freeware for the use of the engineering community. The developed computer tool is designed based on the weights and biases of the hidden layer and the output layer of the proposed network. These weights and biases are the numeric values extracted from the proposed network and are embedded in the tool

during its development.

The computer tool employs the architecture discussed in 2.4. It has one input layer with eleven input parameters that the users need to enter, one hidden layer with twenty-eight neurons, and one output layer, which gives the shear strength. The user interface of the developed computer tool is shown in Fig. 15.

The computer tool executes the network formulations in three main steps. The first step involves the standardization of the input parameters extracted from the proposed network (discussed in 2.5). Afterwards, the weighted sums of all input parameters are calculated using the weights and biases of the hidden layer (discussed in 2.1). These weighted sums are the outputs from the hidden layer. As the final step, the weighted sum of these outputs from the hidden layer is calculated using the weights and biases of the output layer, which is the nominal shear strength of the two-span continuous deep beam.

The developed computer tool is intended to bridge the gap between the research and practical application in shear strength calculation while providing engineers and researchers with a familiar working environment without the need to install and learn a new computer program. The built-in validation system checks for input errors and ensures that the input parameters are within the valid ranges defined in Table 1.

#### 5. Summary and conclusions

This study presented the development of a feed-forward artificial neural network to predict the shear strengths of reinforced concrete two-span continuous deep beams. A comprehensive experimental database is used to train, validate, and test the proposed network for applicability to a wide range of input parameters. The accuracy and reliability of the proposed network are evaluated using a comprehensive set of evaluation metrics. In addition, a computer tool is developed to execute network formulations. The results derived from this study are:



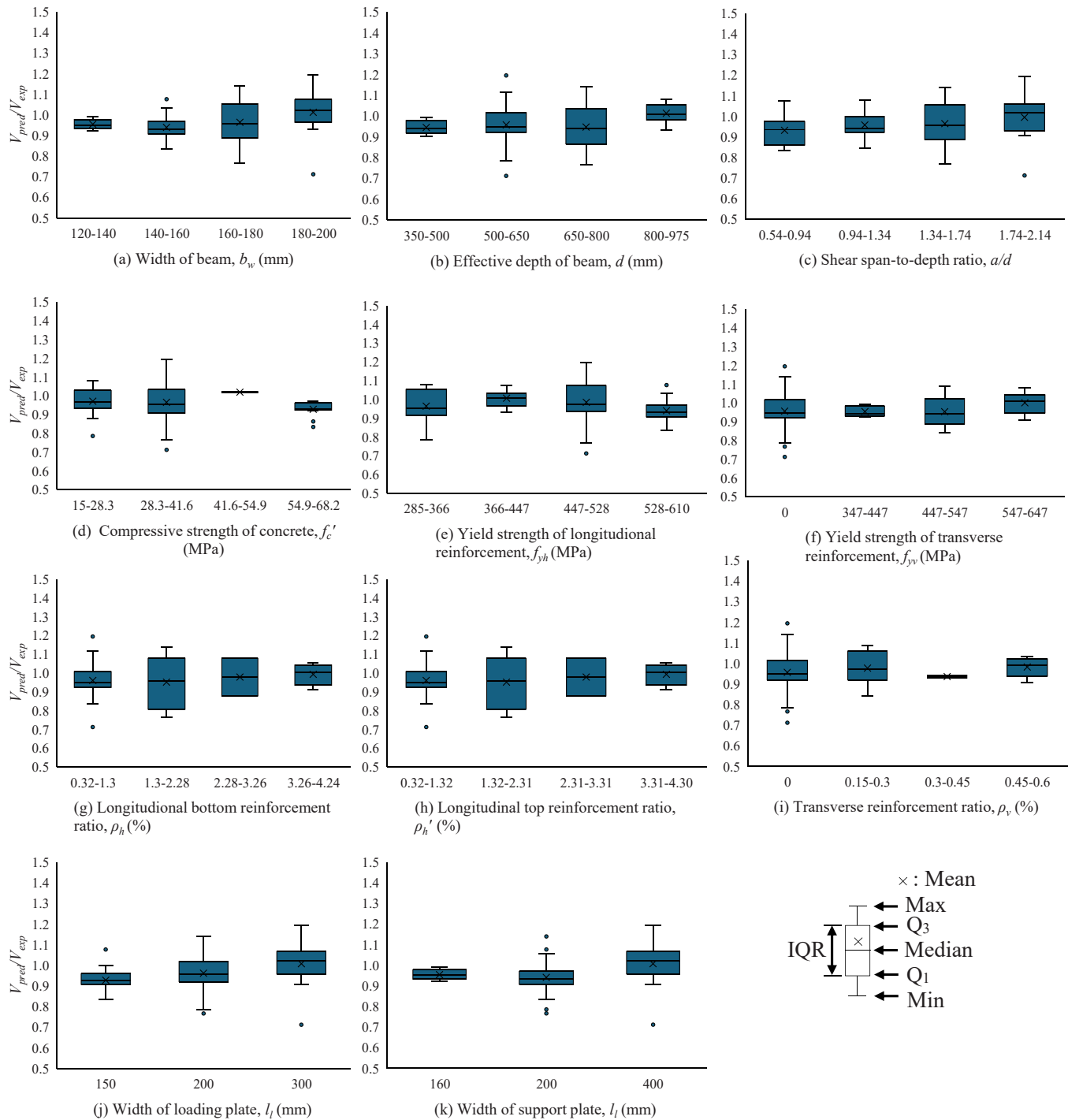


Fig. 13. Comparison of the predicted shear strength across various input parameters range.

Table 3

Error and coefficient of variation comparisons.

ML algorithms	R <sup>2</sup>	MAE (kN)	RMSE (kN)	CV (%)
Proposed network	0.97	32.05	41.26	9.85
Nguyen et al. [23]	0.94	39.30	62.03	23.13
Wang [24]	0.98	17.16	21.02	-*
Feng et al. [25]	0.93	31.81	50.34	7.00
Gandomi et al. [26]	-*	40.99	51.57	-*
Cheng et al. [27]	0.98	-*	13.01	8.00

Note: \* The value is not reported in the respective study.

1. The complex shear behavior of continuous deep beams, influenced by non-linear strain distribution and coexistence of high shear and high moment within the same region makes their accurate shear strength calculations challenging.
2. Feed-forward artificial neural networks can be developed to predict the shear strength of two-span continuous deep beams accurately and rapidly. The database used to train, validate, and test a neural network plays a critical role in identifying the optimum parameters and network architecture. It is recommended to first explore the data to understand its features, detect, and remove any outliers before developing the network. In this study, 10 outliers were found and removed from a database of 150 experimental specimens. Using the

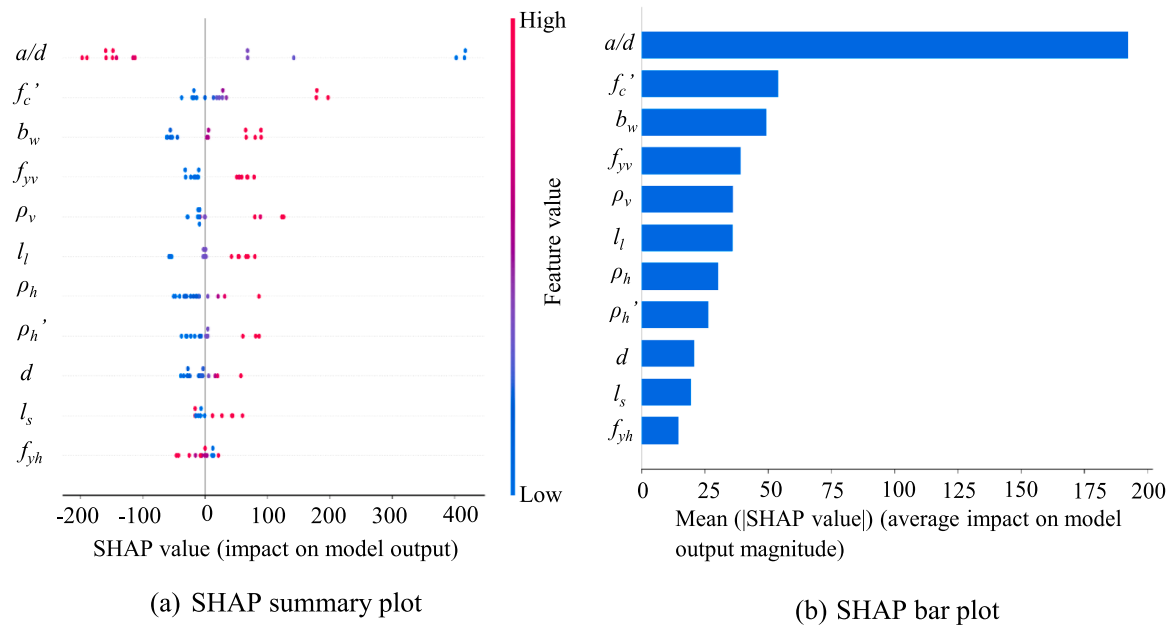


Fig. 14. SHAP summary plot and the relative importance of each feature.

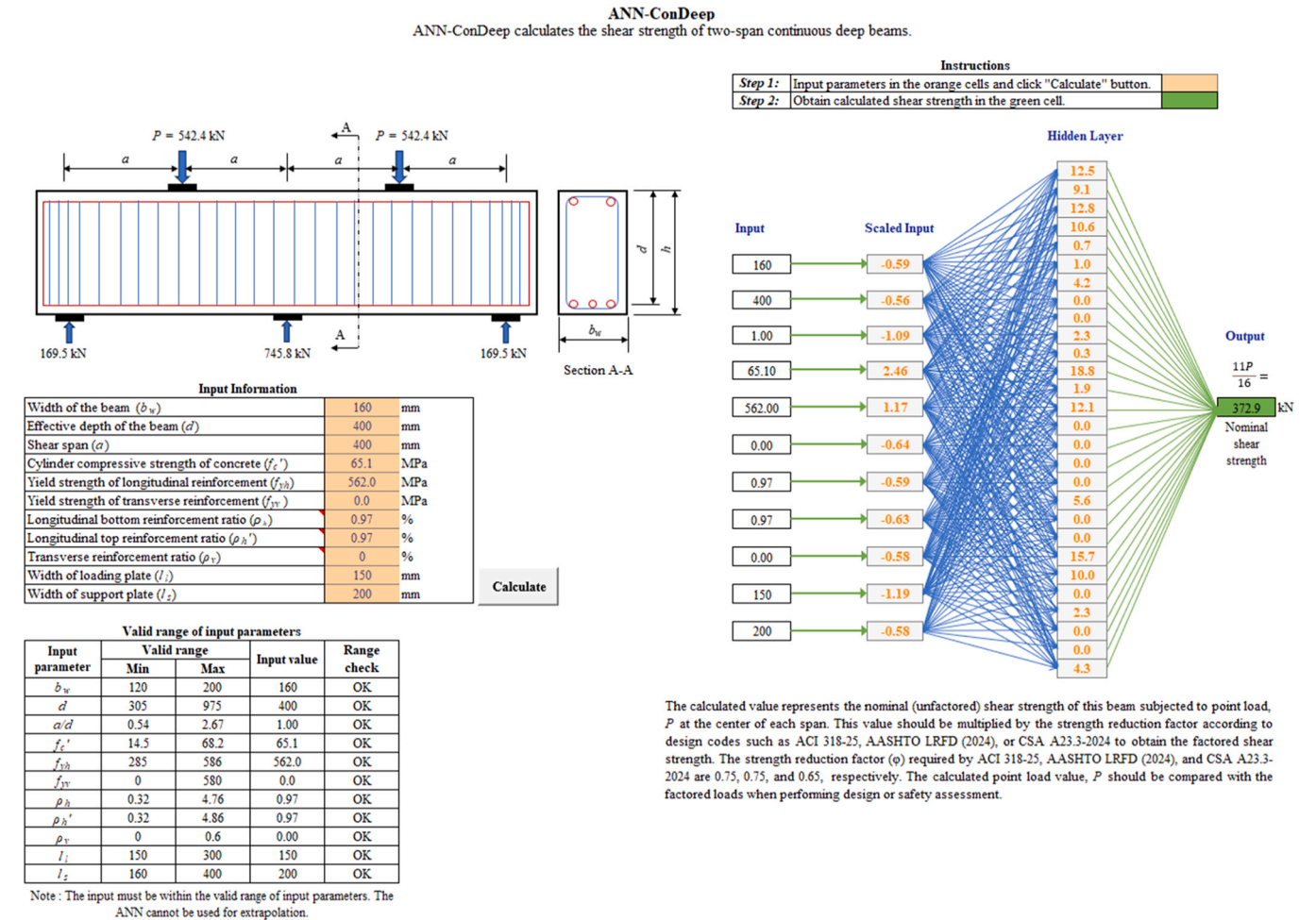


Fig. 15. User interface of the developed computer tool.

- remaining database improved the accuracy and reliability of the proposed neural network.
- The proposed network is shown to predict the shear strength of two-span continuous deep beams accurately, reliably, and rapidly. The predicted-to-experimental shear strength ratios for the 140 specimens provided a mean of 1.00 and a coefficient of variation (CV) of 10.12 %.
  - The proposed network achieves accuracy comparable to previous ML algorithms trained on simply supported deep beams. This emphasizes the network's robustness in handling complex structural behavior and supports its potential for future enhancement through ensemble learning or database expansion.
  - SHAP analysis can effectively improve the understanding of the networks and provide confidence in the machine learning-based predictions by analyzing the influence of parameters on the network's output.
  - SHAP analysis revealed that the shear span-to-depth ratio ( $a/d$ ) had the strongest negative influence on the shear strength predictions of the proposed network, while concrete compressive strength ( $f_c'$ ) showed a significant positive impact. A similar relation is obtained from the correlation coefficient analysis, providing evidence that the network has captured meaningful structural relationships and learned the underlying patterns correctly.
  - The developed computer tool transfers the research results to engineers and researchers and enables them to accurately and rapidly predict the shear strength of the two-span continuous deep beams.

- Future studies could perform structural testing of continuous deep beams with different span lengths and design parameters. The experimental data available in the literature for continuous deep beams lags greatly behind those for simply supported ones.
- Future ML studies should develop computer tools to enable the community to use the proposed algorithms. It is challenging, and sometimes impossible, to use the ML algorithms proposed in literature for the specimens other than those contained in the experimental database used in each study.

#### CRedit authorship contribution statement

**Prativa Pathak:** Data curation, Formal analysis, Investigation, Methodology, Validation, Visualization. **Serhan Guner:** Conceptualization, Funding acquisition, Project administration, Resources, Supervision, Writing – review & editing.

#### Funding sources

This research did not receive any specific grant from funding agencies in the public, commercial, or not-for-profit sectors.

#### Declaration of Competing Interest

No Conflict of Interest.

## Appendix A. . Experimental database

The experimental database compiled for the development of the proposed feed-forward neural network (FFNN) is presented in Table A.1. It comprises 150 experimental beam specimens, all of which exhibited shear-critical behavior, compiled from eight research studies. The first row of Table A.1 presents the input parameters which include the width of the beam ( $b_w$ ), the effective depth of the beam ( $d$ ), the shear span-to-depth ratio ( $a/d$ ), the compressive strength of concrete ( $f_c'$ ), the yield strength of longitudinal and transverse reinforcement ( $f_{yh}$  and  $f_{yv}$ ), the longitudinal top and bottom reinforcement ratio ( $\rho_h'$  and  $\rho_h$ ), the transverse reinforcement ratio ( $\rho_v$ ), the width of loading plate ( $l_l$ ), the width of support plate ( $l_s$ ), and the ratio of the shear strength predicted by the proposed network to the experimental shear strength ( $V_{pred}/V_{exp}$ ). The ten outliers which are not used for training the network are presented with an asterisk (\*).

**Table A.1**  
Experimental database compiled for the development of the proposed network

S.N.	Research studies	Specimens	$b_w$ (mm)	$d$ (mm)	$a/d$	$f_c'$ (MPa)	$f_{yh}$ (MPa)	$f_{yv}$ (MPa)	$\rho_h$ (%)	$\rho_h'$ (%)	$\rho_v$ (%)	$l_l$ (mm)	$l_s$ (mm)	$V_{exp}$ (kN)	$\frac{V_{pred}}{V_{exp}}$
1*	Ashour [31]	CDB1	120	569	1.20	30	500	370	0.66	0.91	0.84	200	160	349.7	
2		CDB2	120	569	1.20	33.1	500	370	0.66	0.91	0.42	200	160	304.9	0.94
3		CDB3	120	569	1.20	22	500	0	0.66	0.91	0	200	160	179.6	0.96
4		CDB4	120	569	1.20	28	500	370	0.66	0.91	0.42	200	160	282.9	0.94
5		CDB5	120	580	1.17	28.7	500	370	0.33	0.33	0.42	200	160	257.1	1.01
6		CDB6	120	371	1.83	22.5	500	347	0.86	0.86	0.47	200	160	155.5	0.99
7		CDB7	120	371	1.83	26.7	500	347	0.86	0.86	0.24	200	160	140	0.92
8		CDB8	120	380	1.79	23.6	500	347	0.5	0.5	0.24	200	160	123.3	0.97
9	Asin [32]	1.0/1/1	150	950	1.26	26.8	586	569	0.32	0.43	0.5	300	400	518	1.01
10		1.0/1/1 (r)	150	950	1.26	29.6	586	569	0.32	0.43	0.5	300	400	529	1.00
11		1.0/1/2	150	950	1.26	27.5	586	569	0.32	0.43	0.38	300	400	495	0.97
12		1.0/1/3	150	950	1.26	25.8	586	569	0.32	0.43	0.22	300	400	388	1.08
13		1.0/2/1	150	975	1.23	25.2	567	569	0.42	0.32	0.5	300	400	588	0.88
14		1.0/2/2	150	975	1.23	28.2	567	569	0.42	0.32	0.38	300	400	469	1.02
15		1.0/2/3	150	975	1.23	30.4	567	569	0.42	0.32	0.22	300	400	422	1.00
16		1.5/1/1	150	575	2.09	29.6	567	569	0.73	0.95	0.5	300	400	402	0.91
17	Mihaylov et al. [35]	1.5/1/1*	150	575	2.09	29.9	567	581	0.73	0.95	0.48	300	400	348	1.03
18		1.5/1/2	150	575	2.09	28.9	567	569	0.73	0.95	0.38	300	400	347	0.93
19		1.5/1/3	150	575	2.09	25.9	567	569	0.73	0.95	0.22	300	400	261	1.02
20		1.5/2/1	150	550	2.18	27.8	567	569	0.95	0.73	0.5	300	400	375	0.94
21		1.5/2/2	150	550	2.18	26	567	569	0.95	0.73	0.38	300	400	339	0.92
22		1.5/2/3	150	550	2.18	28.5	567	569	0.95	0.73	0.22	300	400	246	1.04
23*		CDB1 E	300	1094	1.62	29.7	422	490	0.91	0.91	0.2	300	300	813.4	
24*		CDB1 W	300	1094	1.62	29.7	422	490	0.91	0.91	0.2	300	300	916.7	

(continued on next page)

Table A.1 (continued)

S.N.	Research studies	Specimens	$b_w$ (mm)	$d$ (mm)	$a/d$	$f_c'$ (MPa)	$f_{yh}$ (MPa)	$f_{yv}$ (MPa)	$\rho_h$ (%)	$\rho_h'$ (%)	$\rho_v$ (%)	$l_t$ (mm)	$l_s$ (mm)	$V_{exp}$ (kN)	$\frac{V_{pred}}{V_{exp}}$
25	Moody et al. [30]	I-g	178	305	2.67	30.5	316	0	0.95	0.97	0	203	203	133.4	1.12
26		I-h	178	305	2.67	24.4	328	0	1.48	1.51	0	203	203	132	1.08
27		I-i	178	305	2.67	22.9	328	0	2.1	2.14	0	203	203	146.8	0.95
28		I-1a	178	305	2.67	17.3	316	0	2.86	2.92	0	203	203	114.2	1.16
29		I-1b	178	305	2.67	19.3	316	0	2.86	2.92	0	203	203	129	1.03
30		I-2a	178	305	2.67	16.3	294	0	3.76	3.84	0	203	203	111.2	1.15
31		I-2b	178	305	2.67	18.8	294	0	3.76	3.84	0	203	203	140.9	0.96
32		I-2c	178	305	2.67	26.1	294	0	3.76	3.84	0	203	203	139.4	1.15
33		I-3a	178	305	2.67	15.8	315	0	4.76	4.86	0	203	203	132	1.08
34		I-3b	178	305	2.67	20.5	315	0	4.76	4.86	0	203	203	149.8	1.06
35		I-j	178	305	2.67	33.4	328	0	1.48	1.51	0	203	203	155.7	0.98
36		I-k	178	305	2.67	26.6	328	0	2.1	2.14	0	203	203	161.6	0.88
37		I-4a	178	305	2.67	29.8	316	0	2.86	2.92	0	203	203	163.1	0.97
38		I-4b	178	305	2.67	27.9	316	0	2.86	2.92	0	203	203	132	1.15
39		I-5a	178	305	2.67	28	294	0	3.76	3.84	0	203	203	177.9	0.94
40		I-5b	178	305	2.67	27.9	294	0	3.76	3.84	0	203	203	163.1	1.03
41		I-6a	178	305	2.67	31.4	315	0	4.76	4.86	0	203	203	170.5	1.15
42		I-6b	178	305	2.67	24.6	315	0	4.76	4.86	0	203	203	177.9	0.97
43		I-l	178	305	2.67	35.2	328	0	1.48	1.51	0	203	203	158.7	1.03
44		I-m	178	305	2.67	30.3	328	0	2.1	2.14	0	203	203	155.7	0.98
45		I-7a	178	305	2.67	33	316	0	2.86	2.92	0	203	203	170.5	0.98
46		I-7b	178	305	2.67	34.5	316	0	2.86	2.92	0	203	203	148.3	1.15
47		I-8a	178	305	2.67	33	294	0	3.76	3.84	0	203	203	215	0.87
48		I-8b	178	305	2.67	32.3	294	0	3.76	3.84	0	203	203	163.1	1.14
49		I-9a	178	305	2.67	36.3	315	0	4.76	4.86	0	203	203	192.8	1.11
50		I-9b	178	305	2.67	32.1	315	0	4.76	4.86	0	203	203	192.8	1.03
51		I-n	178	305	2.67	36.1	328	0	1.48	1.51	0	203	203	175	0.95
52		I-o	178	305	2.67	34.8	328	0	2.1	2.14	0	203	203	189.8	0.87
53		I-p	178	305	2.67	41.2	292	0	2.86	2.92	0	203	203	197.2	1.03
54		I-q	178	305	2.67	33.6	285	0	3.76	3.84	0	203	203	192.8	1.01
55		I-r	178	305	2.67	40.9	298	0	4.76	4.86	0	203	203	207.6	1.15
56		II-a	178	533	1.52	26.3	316	0	0.54	0.55	0	203	203	192.8	0.97
57		II-b	178	533	1.52	25.6	300	0	0.84	0.85	0	203	203	215	0.95
58		II-c	178	533	1.52	27.9	290	0	1.2	1.21	0	203	203	249.1	0.93
59		II-d	178	533	1.52	23.7	286	0	1.63	1.65	0	203	203	311.4	0.79
60		II-17a	178	533	1.52	18.3	294	0	2.15	2.18	0	203	203	278.8	0.95
61		II-17b	178	533	1.52	20.7	294	0	2.15	2.18	0	203	203	252.1	1.05
62		II-18a	178	533	1.52	15	315	0	2.72	2.75	0	203	203	326.2	0.88
63		II-18b	178	533	1.52	18.6	315	0	2.72	2.75	0	203	203	266.9	1.08
64		II-19a	178	533	1.52	20.9	313	0	3.46	3.5	0	203	203	357.3	0.91
65		II-19b	178	533	1.52	22.3	313	0	3.46	3.5	0	203	203	324.7	1.01
66		II-20a	178	533	1.52	19.9	302	0	4.24	4.3	0	203	203	348.4	0.79
67		II-20b	178	533	1.52	20.4	302	0	4.24	4.3	0	203	203	369.2	1.00
68		VI-a	178	305	2.67	28.2	316	0	0.95	0.97	0	203	203	102.8	1.41
69		VI-b	178	305	2.67	28.7	344	0	1.48	1.51	0	203	203	172.1	0.85
70		VI-c	178	305	2.67	24.7	328	0	2.1	2.14	0	203	203	146.8	0.96
71		VI-d	178	305	2.67	26.9	290	0	2.86	2.92	0	203	203	157.5	0.99
72		VI-e	178	305	2.67	28.4	285	0	3.76	3.84	0	203	203	170.8	1.02
73		VI-f	178	305	2.67	38.4	328	0	2.1	2.14	0	203	203	186.8	0.94
74		VI-g	178	305	2.67	38.1	290	0	2.86	2.92	0	203	203	173.5	1.10
75		VI-h	178	305	2.67	36.5	285	0	3.76	3.84	0	203	203	206.8	1.00
76		VI-i	178	305	2.67	41.5	314	0	4.76	4.86	0	203	203	194.8	1.20
77	Rogowsky et al. [9]	3/1.0 T1	200	975	1.13	28.9	380	573	0.46	0.63	0.15	300	400	685	1.01
78*		3/1.0 T2	200	975	1.13	28.9	380	573	0.46	0.63	0.15	300	400	764	
79		4/1.0 T1	200	975	1.13	28.5	380	0	0.46	0.63	0	300	400	663	0.96
80		4/1.0 T2	200	975	1.13	28.5	380	0	0.46	0.63	0	300	400	618	1.03
81		5/1.0 T1	200	975	1.13	36.9	403	573	0.46	0.63	0.6	300	400	875	1.01
82		5/1.0 T2	200	975	1.13	36.9	403	573	0.46	0.63	0.6	300	400	834	1.06
83		6/1.0 T1	200	975	1.13	35.8	403	0	0.46	0.63	0	300	400	635	1.02
84		6/1.0 T2	200	975	1.13	35.8	403	0	0.46	0.63	0	300	400	605	1.07
85*		7/1.0 T1	200	975	1.13	34.5	403	0	0.46	0.63	0	300	400	418	
86		7/1.0 T2	200	975	1.13	34.5	403	0	0.46	0.63	0	300	400	695	0.93
87		3/1.5 T1	200	545	2.02	14.5	456	573	0.92	1.12	0.19	300	400	242	1.22
88		3/1.5 T2	200	545	2.02	14.5	456	573	0.92	1.12	0.19	300	400	287	1.03
89		4/1.5T1	200	545	2.02	32.5	456	0	0.92	1.12	0	300	400	206	1.19
90		4/1.5T2	200	545	2.02	32.5	456	0	0.92	1.12	0	300	400	232	1.06
91		5/1.5 T1	200	545	2.02	39.6	460	573	0.92	1.12	0.6	300	400	565	1.03
92		5/1.5 T2	200	545	2.02	39.6	460	573	0.92	1.12	0.6	300	400	566	1.03
93		6/1.5 T1	200	545	2.02	45	460	0	0.92	1.12	0	300	400	256	1.02
94		6/1.5 T2	200	545	2.02	45	460	0	0.92	1.12	0	300	400	258	1.02
95		7/1.5 T1	200	545	2.02	30.4	456	0	0.92	1.12	0	300	400	222	1.12
96		7/1.5 T2	200	545	2.02	30.4	456	0	0.92	1.12	0	300	400	348	0.71
97		8/1.5 T1	200	545	2.02	37.2	456	573	0.92	1.12	0.19	300	400	339	1.07
98		8/1.5 T2	200	545	2.02	37.2	456	573	0.92	1.12	0.19	300	400	382	0.95

(continued on next page)

Table A.1 (continued)

S.N.	Research studies	Specimens	$b_w$ (mm)	$d$ (mm)	$a/d$	$f_c'$ (MPa)	$f_{yh}$ (MPa)	$f_{yv}$ (MPa)	$\rho_h$ (%)	$\rho_h'$ (%)	$\rho_v$ (%)	$l_i$ (mm)	$l_s$ (mm)	$V_{exp}$ (kN)	$\frac{V_{pred}}{V_{exp}}$
99	Yang [33]	3/2.0 T1	200	445	2.47	42.5	460	573	1.12	1.12	0.15	200	400	261	1.00
100		3/2.0 T2	200	445	2.47	42.5	460	573	1.12	1.12	0.15	200	400	277	0.95
101		4/2.0 T1	200	445	2.47	38.3	456	0	1.12	1.12	0	200	400	195	0.98
102		4/2.0 T2	200	445	2.47	38.3	456	0	1.12	1.12	0	200	400	243	0.78
103		5/2.0 T1	200	445	2.47	41.1	460	573	1.12	1.12	0.6	200	400	453	1.02
104		5/2.0 T2	200	445	2.47	41.1	460	573	1.12	1.12	0.6	200	400	456	1.01
105		6/2.0 T1	200	445	2.47	37.4	456	0	1.12	1.12	0	200	400	186	1.03
106		6/2.0 T2	200	445	2.47	37.4	456	0	1.12	1.12	0	200	400	141	1.36
107		7/2.0 T1	200	445	2.47	46.8	460	0	1.12	1.12	0	200	400	185	1.00
108		7/2.0 T2	200	445	2.47	46.8	460	0	1.12	1.12	0	200	400	150	1.24
109		L5NN	160	555	0.54	34.2	562	0	0.97	0.97	0	150	200	456	1.00
110		L5NS	160	555	0.54	34.2	562	483	0.97	0.97	0.3	150	200	475	1.08
111		L5NT	160	555	0.54	34.2	562	483	0.97	0.97	0.6	150	200	512	1.18
112		L5SN	160	555	0.54	34.2	562	0	0.97	0.97	0	150	200	537	0.85
113		L5SS	160	555	0.54	34.2	562	483	0.97	0.97	0.3	150	200	607	0.84
114*		L5TN	160	555	0.54	34.2	562	0	0.97	0.97	0	150	200	640	
115		L10NN	160	555	1.08	32.1	562	0	0.97	0.97	0	150	200	264	0.92
116		L10NS	160	555	1.08	32.1	562	483	0.97	0.97	0.3	150	200	348	0.92
117		L10NT	160	555	1.08	32.1	562	483	0.97	0.97	0.6	150	200	446	0.96
118		L10SN	160	555	1.08	32.1	562	0	0.97	0.97	0	150	200	265	0.92
119		L10SS	160	555	1.08	32.1	562	483	0.97	0.97	0.3	150	200	352	0.91
120		L10TN	160	555	1.08	32.1	562	0	0.97	0.97	0	150	200	288	0.85
121		H6NN	160	555	0.65	65.1	562	0	0.97	0.97	0	150	200	633	0.93
122		H6NS	160	555	0.65	65.1	562	483	0.97	0.97	0.3	150	200	683	0.94
123		H6NT	160	555	0.65	65.1	562	483	0.97	0.97	0.6	150	200	757	0.97
124		H6SN	160	555	0.65	65.1	562	0	0.97	0.97	0	150	200	703	0.83
125*		H6SS	160	555	0.65	65.1	562	483	0.97	0.97	0.3	150	200	799	
126*		H6TN	160	555	0.65	65.1	562	0	0.97	0.97	0	150	200	852	
127	H10NN	160	555	1.08	68.2	562	0	0.97	0.97	0	150	200	372	0.96	
128*	H10NS	160	555	1.08	68.2	562	483	0.97	0.97	0.29	150	200	413		
129	H10NT	160	555	1.08	68.2	562	483	0.97	0.97	0.60	150	200	637	0.97	
130	H10SN	160	555	1.08	68.2	562	0	0.97	0.97	0	150	200	387	0.92	
131	H10SS	160	555	1.08	68.2	562	483	0.97	0.97	0.3	150	200	492	0.97	
132	H10TN	160	555	1.08	68.2	562	0	0.97	0.97	0	150	200	388	0.92	
133	Yang [34]	L5-40	160	355	0.56	32.4	562	0	1.01	1.01	0	150	200	408	0.95
134		L5-60	160	555	0.54	32.4	562	0	0.97	0.97	0	150	200	473	0.96
135		L5-72	160	653	0.55	32.4	562	0	1.1	1.1	0	150	200	492	0.99
136		L10-40	160	355	1.13	32.1	562	0	1.01	1.01	0	150	200	202	0.90
137		L10-60	160	555	1.08	32.1	562	0	0.97	0.97	0	150	200	262	0.93
138		L10-72	160	653	1.10	32.1	562	0	1.1	1.1	0	150	200	301	0.91
139		H6-40	160	355	0.68	65.1	562	0	1.01	1.01	0	150	200	591	0.93
140		H6-60	160	555	0.65	65.1	562	0	0.97	0.97	0	150	200	633.5	0.93
141		H6-72	160	653	0.66	65.1	562	0	1.1	1.1	0	150	200	696.5	0.86
142		H10-40	160	355	1.13	67.5	562	0	1.01	1.01	0	150	200	335	1.06
143		H10-60	160	555	1.08	68.2	562	0	0.97	0.97	0	150	200	372.5	0.96
144		H10-72	160	653	1.10	67.5	562	0	1.1	1.1	0	150	200	392.5	0.94
145	Zhang et al. [8]	TCDB 1-1	180	687	1.46	35.6	515	0	1.86	1.86	0	200	200	473	0.77
146		TCDB 1-2	180	687	1.46	36.1	515	0	1.86	1.86	0	200	200	377	0.96
147		TCDB 1-3	180	687	1.46	38	515	0	1.86	1.86	0	200	200	322	1.14
148*		TCDB 2-1	180	687	1.46	38.9	515	0	1.86	1.86	0.28	200	200	612	
149		TCDB 2-2	180	687	1.46	39.3	515	526	1.86	1.86	0.28	200	200	581	0.77
150		TCDB 2-3	180	687	1.46	38.5	515	526	1.86	1.86	0.28	200	200	460	0.94
														Mean	1.00
														CV	10.12 %

## Data availability

Some or all data, models, or code that support the findings of this study are available from the corresponding author upon reasonable request.

## References

- [1] ACI Committee 318 (2025) "Building Code for Structural Concrete-code Requirements and Commentary," American Concrete Institute, Farmington Hills, MI, USA.
- [2] AASHTO LRFD (2020) "AASHTO LRFD Bridge Design Specifications, Ninth edition," Customary US units, American Association of State Highway and Transportation Officials, Washington, DC, USA, 1904 pp.
- [3] CSA A23.3 (2024) "Design of Concrete Structures," Canadian Standards Association, Mississauga, ON, Canada, 341 pp.
- [4] IS 456 (2000) "Indian Standard Code of Practice Plain and Reinforced Concrete," Bureau of Indian Standards, Manak Bhavan, New Delhi, India, 100 pp.
- [5] Cement Association of Canada (2006) "Concrete Design Handbook, Third edition," Cement Association of Canada, Ottawa, ON, Canada.
- [6] Peng F, Cai Y, Yi W, Xue W. Shear behavior of Two-Span continuous concrete deep beams reinforced with GFRP Bars. Eng Struct 2023;290(116367). <https://doi.org/10.1016/j.engstruct.2023.116367>.
- [7] Chen H, Yi W-J, Ma ZH, Hwang H-J. Shear strength of reinforced concrete simple and continuous deep Beams. ACI Struct J 2019;116(6):31–40. <https://doi.org/10.14359/51718003>.
- [8] Zhang N, Tan KH. Effects of support settlement on continuous deep beams and STM modeling. Eng Struct 2010;32(2):361–72. <https://doi.org/10.1016/j.engstruct.2009.09.019>.
- [9] Rogowsky DM, Macgregor JG, Ong SY. Tests of reinforced concrete deep Beams. ACI Struct J 1986;83(4):614–23. <https://doi.org/10.7939/R3RX93D7D>.
- [10] Abbood IS. Strut-and-Tie model and its applications in reinforced concrete deep beams: a comprehensive review. Case Stud Constr Mater 2023;19(e02643). <https://doi.org/10.1016/j.cscm.2023.e02643>.



- [11] Baniya P, Guner S. Specialized Strut-And-Tie method for rapid strength prediction of bridge pier Caps. *Eng Struct* 2019;198(109474). <https://doi.org/10.1016/j.engstruct.2019.109474>.
- [12] Zhang J, Sun Y, Li G, Wang Y, Sun J, Li J. Machine-learning-assisted shear strength prediction of reinforced concrete beams with and without Stirrups. *Eng Comput* 2022;38(5). <https://doi.org/10.1007/s00366-020-01076-x>.
- [13] Ma C, Wang W, Wang S, Guo Z, Feng X. Prediction of shear strength of RC slender beams based on interpretable machine Learning. *Structures* 2023;57(105171). <https://doi.org/10.1016/j.istruc.2023.105171>.
- [14] Lee JD, Kang TH-K. Ultimate shear strength prediction for slender reinforced concrete beams without transverse reinforcement using machine learning approach. *ACI Struct J* 2024;121(2):87–98.
- [15] Ho VC, Nguyen TH, Nguyen TQ, Nguyen DD. Application of neural networks for the estimation of the shear strength of circular RC Columns. *Eng Technol Appl Sci Res* 2022;12(6):9409–13. <https://doi.org/10.48084/etasr.5245>.
- [16] Phan V-T, Tran V-L, Nguyen V-Q, Nguyen D-D. Machine learning models for predicting shear strength and identifying failure modes of rectangular RC Columns. *Buildings* 2022;12(10):1493. <https://doi.org/10.3390/buildings12101493>.
- [17] Alagundi S, Palanisamy T. Neural network prediction of joint shear strength of exterior beam-column joint. *Structures* 2022;37:1002–18. <https://doi.org/10.1016/j.istruc.2022.01.013>.
- [18] Haido JH. Prediction of the shear strength of RC beam-column joints using new ANN formulations. *Structures* 2022;38:1191–209. <https://doi.org/10.1016/j.istruc.2022.02.046>.
- [19] Suwal N, Guner S. Plastic hinge modeling of reinforced concrete Beam-Column joints using artificial neural Networks. *Eng Struct* 2024;298:117012. <https://doi.org/10.1016/j.engstruct.2023.117012>.
- [20] Almeida SA, Guner S. Review of artificial neural network and a new Feed-Forward network for anchorage analysis in cracked Concrete. *Concr Ind Era Artif Intell* 2021;350(5):54–68. ([https://www.utoledo.edu/engineering/faculty/serhan-guner/docs/JP23\\_Almeida\\_Guner\\_AI\\_Concrete\\_2021.pdf](https://www.utoledo.edu/engineering/faculty/serhan-guner/docs/JP23_Almeida_Guner_AI_Concrete_2021.pdf)).
- [21] Goh ATC. Prediction of ultimate shear strength of deep beams using neural Networks. *ACI Struct J* 1995;92(1):28–32. (<https://www.concrete.org/publications/internationalconcreteabstractsportal.aspx?m=details&ID=1470>).
- [22] Sanad A, Saka MP. Prediction of ultimate shear strength of reinforced concrete deep beams using neural Networks. *J Struct Eng* 2001;127(7):818–28. [https://doi.org/10.1061/\(ASCE\)0733-9445\(2001\)127:7\(818\)](https://doi.org/10.1061/(ASCE)0733-9445(2001)127:7(818)).
- [23] Nguyen KL, Trinh HT, Nguyen TT, Nguyen HD. Comparative study on the performance of different machine learning techniques to predict the shear strength of RC deep beams: model selection and industry Implications. *Expert Syst Appl* 2023;230(120649). <https://doi.org/10.1016/j.eswa.2023.120649>.
- [24] Wang H, Zhang C, Wu H. Shear capacity prediction model of deep beam based on new hybrid intelligent algorithm. *Buildings* 2023;13(6):1395.
- [25] Feng DC, Wang WJ, Mangalathu S, Hu G, Wu T. Implementing ensemble learning methods to predict the shear strength of RC deep beams with/without web reinforcements. *Eng Struct* 2021;235:111979. <https://doi.org/10.1016/j.engstruct.2021.111979>.
- [26] Gandomi AH, Yun GJ, Alavi AH. An evolutionary approach for modeling of shear strength of RC deep Beams. *Mater Struct* 2013;46:2109–19. (<https://link.springer.com/article/10.1617/s11527-013-0039-z>).
- [27] Cheng M-Y, Cao M-T. Evolutionary multivariate adaptive regression splines for estimating shear strength in Reinforced-Concrete deep beams. *Eng Appl Artif Intell* 2014;28:86–96.
- [28] Chou J-S, Ngo N-T, Pham A-D. Shear strength prediction in reinforced concrete deep beams using Nature-Inspired metaheuristic support vector Regression. *J Comput Civ Eng* 2016;30(1):04015002. [https://doi.org/10.1061/\(ASCE\)CP.1943-5487.0000547](https://doi.org/10.1061/(ASCE)CP.1943-5487.0000547).
- [29] Bircanoğlu C, Arica N. A comparison of activation functions in artificial neural networks. 26th Signal Process Commun Appl Conf (SIU) 2018:1–4. <https://doi.org/10.1109/SIU.2018.8404724>.
- [30] Moody KG, Viest IM, Elstner RC, Hognestad E. Shear strength of reinforced concrete beams part 2—Tests of restrained beams without web reinforcement. *ACI J Proc* 1955;51(1):417–34.
- [31] Ashour AF. Tests of reinforced concrete continuous deep beams. *ACI Struct J* 1997;94(1):3–12. (<https://www.concrete.org/publications/internationalconcreteabstractsportal/m/details/id/455>).
- [32] Asin, M. (1999) The Behavior of Reinforced Concrete Continuous Deep Beams, Doctoral Thesis, Delft University Press, Delft, Netherlands, 167 pp.
- [33] Yang KH, Chung HS, Ashour AF. Influence of shear reinforcement on reinforced concrete continuous deep Beams. *ACI Struct J* 2007;104(4):420–9.
- [34] Yang KH, Chung HS, Ashour AF. Influence of section depth on the structural behavior of reinforced concrete continuous deep Beams. *Mag Concr Res* 2007;59(8):575–86. <https://doi.org/10.1680/mac.2007.59.8.575>.
- [35] Mihaylov BI, Hunt B, Bentz EC, Collins MP. Three-parameter kinematic theory for shear behavior of continuous deep Beams. *ACI Struct J* 2015;112(1):47–58. [https://doi.org/10.1061/\(ASCE\)CC.1943-5614.0000747](https://doi.org/10.1061/(ASCE)CC.1943-5614.0000747).
- [36] Diab AY, Ferche AC. Prediction of tensile properties of Ultra-High-Performance concrete using artificial neural Network. *ACI Struct J* 2024;121(2):57–69. <https://doi.org/10.14359/51740245>.
- [37] Pedregosa, F.; Varoquaux, G.; Gramfort, A.; Michel, V.; Thirion, B.; Grisel, O. et al. (2011) “StandardScaler from Scikit-learn (v1.6.1): Machine learning in Python software,” Python Software Foundation. (<https://scikit-learn.org/stable/modules/generated/sklearn.preprocessing.StandardScaler.html>).
- [38] Ramakrishnan V, Ananthanarayan Y. Ultimate shear strength of deep beams in shear. *ACI J* 1968;65(2):87–98. <https://doi.org/10.14359/7458>.
- [39] Yang KH, Eun HC, Chung HS, Lee ET. Shear characteristics of High-Strength concrete deep beams without shear reinforcement. *Eng Struct* 2003;25(8):1343–52. [https://doi.org/10.1016/S0141-0296\(03\)00110-X](https://doi.org/10.1016/S0141-0296(03)00110-X).
- [40] P. Pathak S. Guner ANN-ConDeep: Artificial Neural Network for Continuous Deep Beams 2025 Excel Spreadsheet, Department of Civil and Environmental Engineering, The University of Toledo Toledo, OH, USA. <https://www.utoledo.edu/engineering/faculty/serhan-guner/spreadsheets.html>.